High-resolution spectroscopy of the 1S-2S transition of atomic hydrogen and deuterium

F. Schmidt-Kaler, D. Leibfried, S. Seel, C. Zimmermann, W. König, M. Weitz, and T. W. Hänsch
Max-Planck-Institut für Quantenoptik, D-85748 Garching, Germany
(Received 10 June 1994)

Two-photon spectroscopy of the hydrogen 1S-2S transition in a cold atomic beam has reached a resolution $\Delta\nu/\nu$ of 1 part in 10^{11} in hydrogen and 7 parts in 10^{12} in deuterium. The hydrogen and deuterium 1S-2S transition frequencies have been determined with a precision of 1 part in 10^{11}. This leads to an accurate value for the Rydberg constant, while the 1S Lamb shift and the isotope shift are determined with order of magnitude improvements over previous measurements. We describe in detail the 1S-2S spectrometer, calculate the line shape of the resonance, and compare it to the experimental data.

PACS number(s): 32.30.Jc, 42.62.Fi, 42.50.Wm, 06.20.Jr

I. INTRODUCTION

High-resolution spectroscopy of simple atoms permits confrontations between experiment and fundamental physical theories. Precise absolute measurements and comparisons between different transition frequencies yield accurate values for fundamental constants and allow stringent tests of basic physical concepts such as, for instance, the quantum electrodynamic theory of the Lamb shift [1]. Recently dramatic advances in measurement precision occurred due to the development of new techniques for synthesizing, stabilizing, and measuring optical frequencies [2]. This enhances interest in narrow atomic transitions, among which the 1S-2S transitions of hydrogen (and deuterium) is one of the most intriguing candidates. It has an extremely small natural linewidth of 1.3 Hz and may be observed Doppler-free by two-photon excitation near 243 nm. In our experiments we now have reached a resolution $\Delta\nu/\nu$ of 1 part in 10^{11} in a cold atomic beam. With this result the 1S-2S transition is the best resolved resonance in atomic hydrogen by far [3]. We give here a detailed description of the 1S-2S two-photon spectrometer which had been used in a series of recent precision measurements [4–6].

To avoid collisions we excite the 1S-2S transition in an atomic beam such that transit time broadening and the relativistic Doppler effect remain the dominant broadening mechanisms. Both have been reduced by cooling the beam nozzle with liquid nitrogen or liquid helium. Inelastic wall collisions inside the nozzle lead to a thermal beam with a temperature down to a few kelvin. The resolution possible with this spectrometer made it necessary to improve the monochromatic laser source which we used in former studies of the 1S-2S transition [7]. A special ultrastable high-finesse Fabry-Pérot resonator has been added to the dye laer system near 486 nm and an efficient and reliable second-harmonic generation stage has been developed for the present experiments.

First we give a detailed description of the 1S-2S spectrometer including the laser system near 486 nm, the frequency-doubling stage for the generation of coherent radiation near 243 nm, and the atomic beam apparatus (Sec. II). We also discuss recent experimental tests of the laser frequency stability. Section III describes the lineshape analysis of the two-photon resonance. We give an approximated analytic expression for the excitation probability of a single atom and calculate the line shape by averaging over the different trajectories and the velocity distribution. Theoretical and experimental line shapes are compared for several different experimental parameters. In Sec. IV we discuss various systematic effects due to electric and magnetic fields, ionization broadening, light shift, and other perturbations. We estimate the ultimate precision possible with our present experimental setup. The Zeeman shift of the 1S-2S transition of hydrogen and deuterium may be studied by applying a weak magnetic field. At field strengths of several gauss all Zeeman sublevels have been resolved and interpreted in terms of the Breit-Rabi equation. In Sec. V we review recent measurements which exploit the ultrahigh resolution of the 1S-2S spectrometer. The 1S Lamb shift has been determined with an accuracy of 7.5 parts in 10^6 [5] which exceeds the precision of the best mesurement of the "classical" 2S Lamb shift [8]. With this result the 1S Lamb shift experiment establishes the current best test of quantum electrodynamics for an atom and complements the well-known measurement of the g factor for a free electron [9]. We have also measured the isotope shift between hydrogen and deuterium which provides information about the nuclear size of simple hadronic systems [4]. With our tabletop experiment, we rival the accuracy of high-energy electron-hadron scattering experiments and are able to observe nuclear properties at low energies which are inaccessible in accelerator experiments. Finally, we describe the measurement of the absolute 1S-2S transition frequency by means of a frequency chain, which is used to determine the hydrogen 1S-2S frequency with help of the cesium time standard [6]. From this experiment we derive a value for the Rydberg constant with an accuracy of 3 parts in 10^{11}, in good agreement with a more recent measurement [10]. These new measurements of the Rydberg constant not only play a key role in the determination of a self-consistent system of fundamental constants, they also provide a new set of reference frequencies throughout the ultraviolet, visible, infrared, and microwave region, since the frequencies of other hydro-

gen transitions may now be calculated with improved accuracy. Finally, we point out that with the resolution now achieved one may even think of experiments to measure small drifts in fundamental constants, as discussed on the basis of grand unified theories [11].

II. THE 1S-2S SPECTROMETER

A. Dye laser

Our laser system is based on a commercial ring dye laser operating at 486 nm with an output power of approximately 500 mW (Coherent CR-699, Coumarin 102). It is pumped by a 5.5-W Kr^+-ion laser (Coherent, Inova 200) (see Fig. 1). To improve the passive frequency stability of the dye laser, the standard dye nozzle is replaced by a commercial high-pressure nozzle (Radiant Dyes, Wermelskirchen, Germany) made of polished stainless steel. It has a slit width of 200 μm and is operated at a pressure of 11.5 bar. In addition, the standard pump mirror mount as well as the original étalon assembly were replaced by commercial substitutes (Radiant Dyes) which allow for more exact and stable adjustment of the pump focus and for separate adjustment of the two étalons inside the laser. As a result the laser output power is enhanced by roughly a factor of 2 with the high-pressure pump and the exact focus adjustment as key points for better performance. We use an air reservoir to damp pressure fluctuations of the dye. Inside the laser cavity the commercial galvomounted Brewster plate, the piezomounted mirror, and an additional electro-optical modulator (EOM) (Gsänger PM 25) compensate frequency fluctuations up to about 1.5 MHz. If the laser is stabilized to the coherent reference cavity by the commercial electronics, we measure a frequency jitter of 1.5 MHz.

B. Laser frequency stabilization

For high-resolution spectroscopy we require a narrow laser bandwidth on the order of 1 kHz. Thus we lock the laser frequency to a very stable external reference cavity by means of a radio-frequency sideband modulation technique [12,13]. For this purpose a small part of the 486-nm laser light is phase modulated with an electro-optical modulator (LM 0202, Gsänger) which is driven by a function generator (Hewlett-Packard 8116A) at 21.1 MHz. A 5-W amplifier (Kalmus Engineering, model 302F) enhances the output of the function generator, yielding a modulation index of 50%.

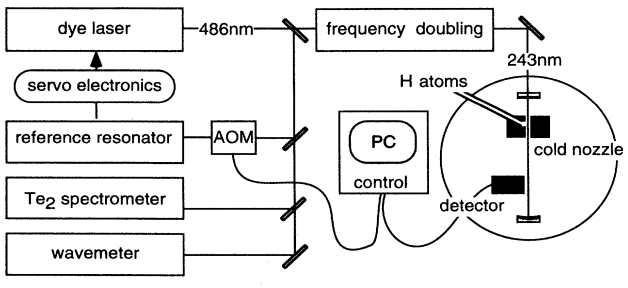

FIG. 1. Schematic overview of the experimental setup. The dye laser is stabilized to the reference cavity. The light frequency is doubled in order to excite the 1S-2S two-photon resonance in an atomic beam of hydrogen or deuterium.

Proper mode matching into a TEM_{00} mode of the reference cavity is achieved with a telescope formed by two lenses (Fig. 2). Higher-order transverse modes are suppressed by a factor of 10. The radii of the mirrors ($R=-1$ m) and the length of the cavity ($l=0.45$ m) are chosen such that the resonance frequencies of higher-order modes do not coincide with the resonance of the TEM_{00} mode.

The light reflected from the cavity (0.5 mW) is detected by a photodiode (FND 100, EG&G), followed by a current-to-voltage converter. After further amplification (Miteq AM-1299, 1-GHz bandwidth, 40-dB gain) the signal is demodulated with a mixer (SRA 1, Mini Circuits). The resulting error signal is again amplified (BurrBrown 3554, gain approximately equal to 125, 3-dB point approximately equal to 10 MHz) and then split into three paths of different response time. The fast components of frequencies up to 1.5 MHz are directly fed into one electrode of the EOM inside the laser cavity. A high-voltage amplifier (BurrBrown 3584, gain approximately equal to 70, 3-dB point approximately equal to 3 kHz) is used to supply the other electrode of the EOM and controls the intermediate frequency range between 100 and 3 kHz. The slow branch is formed by an amplifier (gain approximately equal to 100, 3-dB point at 300 Hz, Tektronix, AM 502 Differential Amp.) whose output is connected to the commercial laser frequency control box (test point 1 on the differential amplifier board, Coherent CR-699) [14]. In addition we use the error signal from the simultaneously operating commercial laser stabilization and add it to the slow branch of our control scheme. This error signal uses the resonance of a low-finesse cavity and provides an auxiliary signal at large deviations of the laser frequency.

A reliable test for the quality of the servo loop is obtained by recording the beat signal between two different dye lasers locked on the same resonantor. Using a fast photodiode (Antel) we observe a 20-Hz-wide beat note

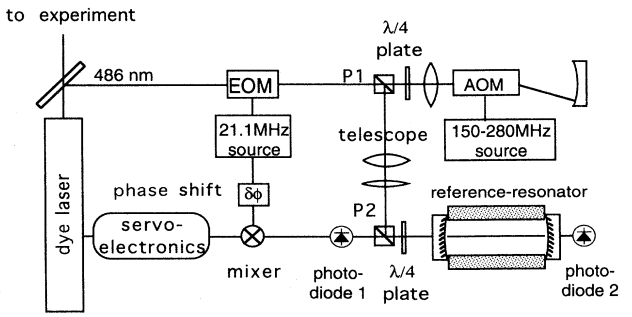

FIG. 2. Scheme of the heterodyne frequency stabilization. FM sidebands are modulated at 21.2 MHz. The frequency is shifted by a tunable AOM in a double-path geometry and coupled into the reference resonator. The carrier phase shift of the reflected light is detected and serves as an error signal for the laser servo loop.

with a resolution bandwidth of 10 Hz. This agrees well with the estimation based on the residual fluctuations of the radio-frequency error signal of 10 Hz within a 100-kHz bandwidth.

To detune the laser frequency we use an acousto-optic modulator (AOM) (Crystal Technology 3200-120) placed between the laser and the reference resonator (Fig. 2). The AOM is driven by an amplified (Kalmus Engineering, model 302F, 5W) high-precision signal generator (Rohde&Schwarz, SMG). After passing a polarizing beam splitter and a quarter wave plate, the light is transmitted through the AOM in first order, resulting in an adjustable frequency shift. The light is reflected back from a curved mirror and passes the AOM a second time. The light frequency is thus shifted by twice the AOM frequency relative to the incoming light. The AOM frequency is controlled by the computer and may be scanned between 140 and 280 MHz providing a tuning range of the laser of 280 MHz.

As a coarse gauge for the laser wavelength we use a commercial wavemeter which is precise up to 1 pm. To find the narrow hydrogen and deuterium resonances it is mandatory to tune the laser to the proper frequency within a range of 10 MHz. This is easily done by observing well-calibrated tellurium resonance lines (i_2 and g_1) using Doppler-free saturation spectroscopy [15] (Fig. 1).

C. Stable reference cavity

Since the laser frequency stability is dominated by the stability of the reference cavity, some care has to be taken in its construction [16]. The cavity consists of two mirrors of gyroscope quality which are optically contacted on the polished front surfaces of a 45-cm-long cylindrical Zerodur spacer of 10 cm diameter. Four longitudinal holes of 10 mm diameter are drilled in the spacer 22 mm off the center and are used for four different resonators. Two of them operate at 486 nm. Additional orthogonal holes allow for evacuation of the free space between the mirrors.

We have measured the finesse of our reference cavity by observing its decay time. We first lock the laser frequency to the resonance of a TEM_{00} mode. After blocking the light in front of the resonator with an acousto-optic modulator we observed the exponential decay of the light emitted through the rear mirror of the cavity. From the 28-μs decay time we determine a finesse of 57 000 corresponding to a linewidth of 5.6 kHz. Both mirrors (substrates, General Optics, Inc.; coating, Ojai Optics, CA) are from the same batch and specified with equal 25-ppm transmission and 25-ppm losses adding up to 75-ppm total round-trip losses (excluding the transmission of the input coupling mirror). From these values we calculate a finesse of 63 000, in reasonable agreement with the measured value. On resonance 75% of the incident light is reflected by the resonator.

The resonator spacer bar is suspended from soft springs inside a vacuum chamber evacuated to a pressure of $< 10^{-8}$ mbar. To minimize acoustical and vibrational noise we use an ion getter pump (Leybold IZ 120) (Fig. 3). The requirements for noise isolation are extreme: Any

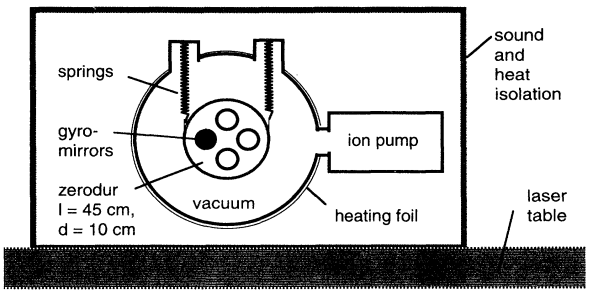

FIG. 3. Mechanical setup of the reference resonator. A rigid Zerodur bar with four longitudinal drilled holes is suspended by weak springs inside a UHV chamber ($p < 10^{-8}$ mbar). The outer surface of the vacuum chamber is temperature stabilized using a heating foil and a hermetically closed box provides additional thermal and acoustic isolation. Gyroscope-quality mirrors are optically contacted to the polished Zerodur spacer.

length fluctuations of the resonator will translate into frequency jitter of the laser with a rate of 140 kHz/Å. Since acoustic waves are effectively isolated by the vacuum, noise is coupled to the resonator bar mainly by the spring suspension which acts like a low pass filter: Noise at frequencies ω higher than the resonance frequency of the suspension Ω are reduced by a factor $1/(\omega - \Omega)^2$. The mechanical resonance Ω of the Zerodur bar suspension system is 1.5 Hz. Around this frequency we expect the main contributions of external noise transported to the resonator. In addition there are transverse string resonances of the suspension springs with eigenfrequencies $\Omega_n = n\Omega\sqrt{M/m}$ (M is the mass of the resonator and m the mass of the spring) [17].

We have measured the beat note between our laser system and a second almost identical dye laser, both stabilized on two different optical resonators on the same spacer (Fig. 4). The width of the beat signal of less than 1 kHz is probably limited by the mechanical oscillations of the Zerodur bar in a transverse bending mode. We suspect that since the holes for the optical resonators are drilled off center through the Zerodur bar, bending modes of the spacer are transformed directly into length variations of the optical resonators. Thus, in the future we will use a center drilled spacer. We have also measured the power spectrum of the light intensity transmitted through one of the resonators, with the laser locked to the second cavity on the same Zerodur bar (Fig. 5). As expected, the resonances of suspension system and string resonances of the springs appear as pronounced peaks at 1.5 Hz and near 120 Hz. For the future we plan to further improve the resonator stabilty by actively damping the motion of the bar. For a genuine measurement of the laser frequency stability we have set up a second 11.5-cm-long completely independent reference cavity (diameter of the Zerodur bar 50 mm). Similar to the 45-cm cavity, it consists of a Zerodur spacer and is placed inside a second vacuum housing. With the laser locked to the 11.5-cm resonator, we tune across the resonance of the 45-cm resonator by means of the AOM and observe the radio-frequency error signal (Fig. 6). This detection method provides a signal whose zero crossing is almost

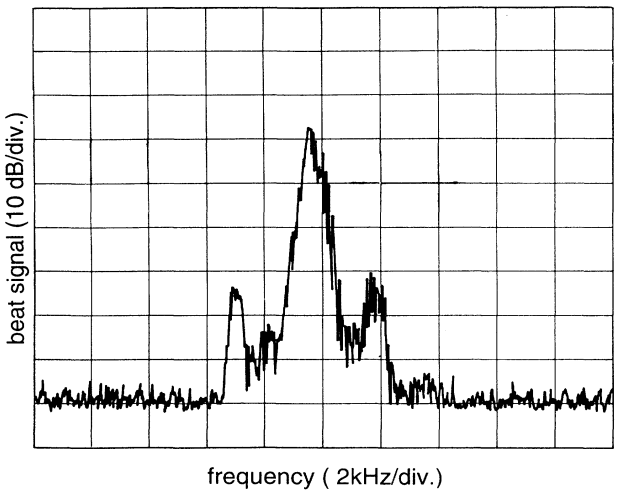

FIG. 4. Measurement of the 45-cm reference cavity's stability. Two lasers near 496 nm are stabilized to different optical reference resonators mounted on the same 45-cm-long Zerodur spacer. The beat note is observed on a photodiode, amplified, and detected on a spectrum analyzer with a resolution bandwidth of 215 Hz and a scan period of 1.4 s. The central peak with a width of less than 1 kHz is probably caused by the bending oscillation of the Zerodur spacer. At 2 kHz we observe the servo bumps of the low-frequency branch of the laser stabilization as sidebands.

independent of laser intensity fluctuations. Thus the distortions of the observed dispersive Lorentzian shape directly reflect the frequency fluctuations of both the lasers. From the noise of the error signal we estimate an absolute laser frequency stabilty of about 2 kHz in our rather noisy laboratory.

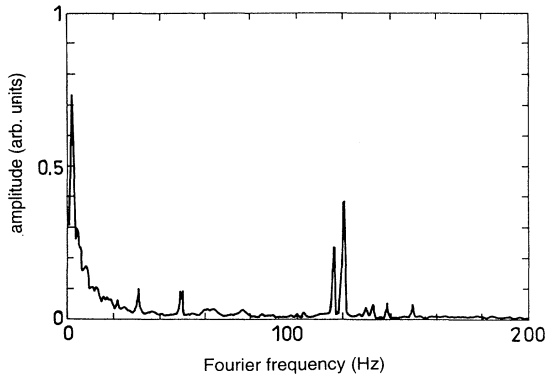

FIG. 5. Fourier spectrum of frequency perturbations. The laser is locked to the reference resonator on the 45-cm Zerodur spacer and tuned across a resonance of a second optical resonator mounted on the same spacer. The transmitted light is detected by a photodiode. We adjust the frequency to the wing of the resonance and record the Fourier transform of the transmission signal. The main perturbations originate from eigenoscillations of the resonator suspension at 1.5 Hz, while at 120 Hz the first string resonance of the springs enhances the noise coupled to the resonator (the different strengths of the two pairs of springs result in two slightly different resonance frequencies).

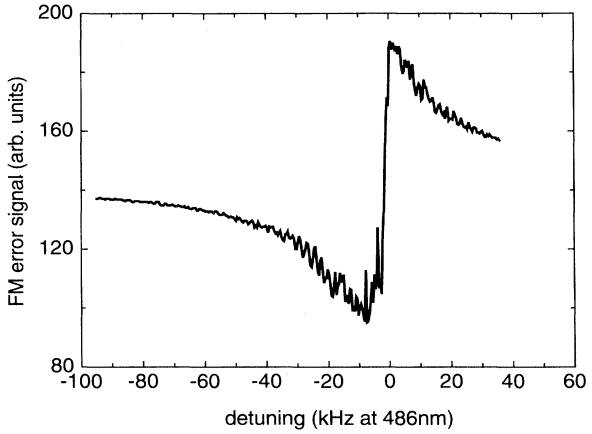

FIG. 6. Radio-frequency error signal. The laser is frequency stabilized to a 11.5-cm-long reference cavity while part of the light is tuned across the resonance of a 45-cm-long reference cavity with an acousto-optic modulator. We observe the radio-frequency error signal of the 45-cm cavity. Distortions on the wings of the dispersive signal are due to oscillatory frequency fluctuations that are mainly due to suspension resonances of the 11.5-cm cavity near 1 Hz. From this signal we estimate the frequency stability of the 45-cm cavity to be better than 2 kHz.

The long-term drift stability of the reference resonator is improved substantially by stabilizing the temperature of the vacuum chamber. We heat the chamber to 27.5 °C by running a current through a thin graphite-coated plastic foil which covers approximately three-quarters of the chambers outside surface. An electronic servo loop controls the current. At the control point the temperature is kept constant within 5 mK. A box made from special wood–lead-rubber–wood sandwich material covers the whole system and serves as additional thermal and acoustical isolation. We observe a frequency drift of the reference cavity of about 10 Hz/s relative to the hydrogen resonance (see also Sec. III).

D. Frequency doubling

From the output of the blue dye laser we couple up to 450 mW into a passive ring resonator which contains a β-barium-borate (BBO) crystal for generation of second-harmonic radiation at 243 nm (Fig. 7). The input coupling mirror (1.8% transmission at 486 nm) and one of the two curved mirrors (piezomounted high reflecting "tweeter" with $R = -75$ mm) are taken from a Coherent dye laser. The second curved mirror ($R = -100$ mm, high reflecting at 486 nm and 95% reflection at 243 nm) also reflects the generated uv light which leaves the resonator through the second flat mirror (85% transmission at 243 nm and high reflecting at 486 nm). Coatings and substrates of the two latter mirrors are custom made (Laser Optics, Garbsen, Germany). The 11.5-mm-long crystal is cut for Brewster angle and 55° type-1 angle tuned phase matching. The optimal focusing of the blue light inside the crystal has been calculated following the theory of Boyd and Kleinman [18]. To determine the theoretically expected second-harmonic yield we have extended the theory to astigmatic optical beams. The beam

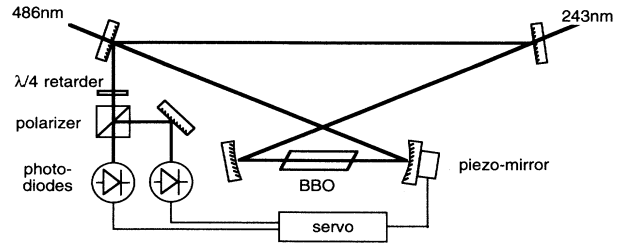

FIG. 7. Enhancement cavity for 486 nm and frequency doubling. A 11.5-mm-long β-barium-borate (BBO) crystal is placed in the focus of a buildup cavity (the beam waist is 19.5 mm). The optical path length between r_1 and r_2 is denoted d_1, while the rest of the round-trip is d_2.

geometry of the resonator is calculated by standard techniques [19], taking into account the astigmatism caused by the curved mirrors and the Brewster crystal. The length of the cavity is adjusted for a beam waist inside the crystal of 19.5 μm corresponding to a confocal parameter $b=4.4$ mm (distance between the curved mirrors via the crystal, $d_1=97.5$ mm; distance between the curved mirrors via the plane mirrors, $d_2=808$ mm). The incident angle on the curved mirrors of 13° is optimized for maximum overlap of the stability range in the azimuthal and vertical plane (Fig. 8).

The finesse is 250, limited by the losses of the mirror coatings. We observe only small additional loses due to the crystal. On resonance about 75% of the incident light is coupled into the cavity and we estimate a power enhancement of the fundamental light by a factor of 60. The position of the mirror is servo controlled (bandwidth 11 kHz) so that the enhancement resonator stays in resonance with the laser. The error signal is generated by analyzing the polarization of the light reflected off the input coupler [20]. With 20-W circulating power inside the cavity we measure 7 mW of uv light behind the uv output coupler. Taking into account reflection and transmission losses for the uv inside the resonator and at the crystal surface (uv polarization is orthogonal to the blue and thus there is no Brewster angle for the generated uv radiation) the generated uv power of 10 mW corresponds to a conversion coefficient of approximately $P_{uv}/P_{blue}^2=2.5\times10^{-5}$. This is three times lower than the theoretically expected value of 8×10^{-5}.

The walkoff inside the β-barium-borate crystal leads to a strong ellipticity and astigmatism of the uv output beam. We use an $f=300$ mm lens, 250 mm behind the uv output coupler, and a tilted concave mirror ($R=-100$ mm, 75° incident angle) to compensate for the beam shape distortion. Roughly 80% of the light intensity is transformed into a Gaussian TEM_{00} mode.

E. uv enhancement cavity

About 5 mW of uv power is coupled into an approximately 25-cm-long standing-wave cavity inside the vacuum chamber of the atomic beam apparatus. The cavity is formed by a flat input coupler (4% tranmission) and a curved ($R=-500$ mm) high reflector (Tec Optics, fluoride coatings) which is mounted on a piezotransducer (Fig. 9). The almost confocal cavity geometry leads to a beam radius of 140 μm, which varies only by 15% in the excitation region. Outside the vacuum chamber an electrooptic phase modulator (Gsänger, LM 0202 Phas/UV, modulation index 50%) generates sidebands at 21.1 MHz necessary to lock the resonator to the frequency of the input light with the radio-frequency heterodyne technique [12,13]. The measured finesse of 97 and the coupling efficiency of 77% lead to an enhancement factor of 24. At optimum conditions we observe 110-mW circulating uv power inside this resonator. In vacuum, the intracavity power slowly decreases to about 90% of the maximum value and then stays constant for hours.

F. Atomic hydrogen beam

Molecular hydrogen from a commercial pressure bottle is cleaned with a palladium leak and dissociated inside a microwave discharge made from an air cooled Pyrex tube (9 mm diameter) and a commercial microwave oscillator (2.45 GHz, 30 W, Oxford Instruments, Microtron 200). The hydrogen atoms are guided in a 10-cm-long Teflon tube (diameter 9 mm) to a nozzle inside the vacuum chamber of the beam apparatus. The chamber is evacuated by a cryopump (diameter 0.5 m, 10^4 liter/s, Leybold

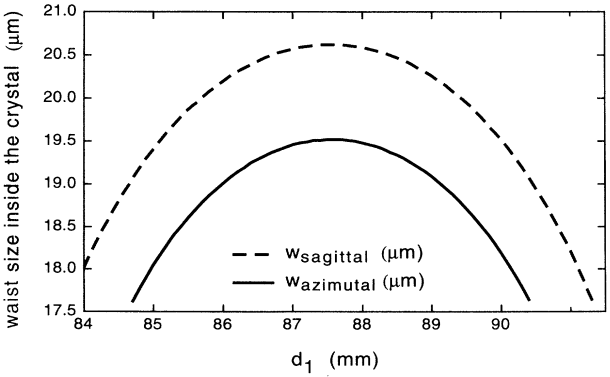

FIG. 8. Beam radius inside the crystal. At an angle of 13° the astigmatism of the Brewster-cut crystal is compensated for by the non-normal reflection of the mirrors r_1 and r_2.

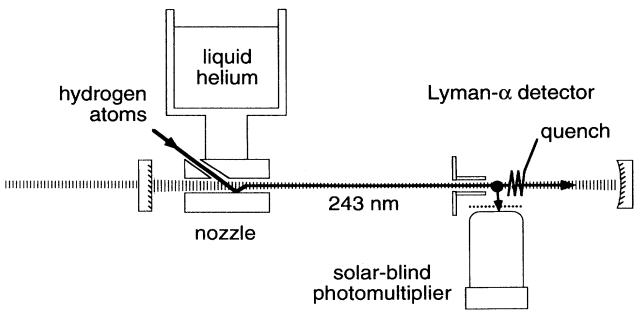

FIG. 9. uv buildup cavity and excitation geometry of the hydrogen and deuterium two-photon transition in a cold thermal beam.

cryopump RPK) which allows for a high flux of 10^{17} hydrogen atoms per second, even at a pressure of 10^{-6} mbar. The nozzle is formed by a hole inside a copper block connected to the bottom of a bath cryostat (Leybold, BBK 150). The cryostat is operated with either liquid nitrogen or liquid helium (see Fig. 9). A slit between the nozzle and the Teflon tube of approximately 0.2 mm width avoids thermal contact between the tube and the nozzle. It also helps to reduce the strong hydrogen recombination on Teflon surfaces which is to be expected at temperatures below 50 K [21]. The efficiency of the gas discharge is monitored by a mass spectrometer (Balzer, QMG 420) attached to the vacuum chamber. From the density ratio of H and H_2 inside the chamber we obtain a lower limit for the dissociation efficiency of 30%. Inside the nozzle the hydrogen atoms (estimated flux 5×10^{17} s^{-1}) lose kinetic energy due to collisions with the wall and form a cold thermal atomic beam. The length (2.5 mm) and the diameter (1.2 mm) of the nozzle were adjusted for an average number of 10 wall collisions. We take this for optimum thermalization on the one hand and moderate recombination probabiilty on the other [21]. However, recombination still turned out to be a serious loss mechanism at temperatures below 20 K.

G. Excitation and detection

The atoms are excited to the metastable $2S$ state on trajectories almost parallel to the standing wave inside the uv cavity. The 11.6-cm-long excitation region is shielded from stray electric fields by a graphite coated net. All surfaces close to the atomic beam are also coated with graphite. The whole vacuum apparatus is surrounded by Helmholtz coils which generate an adjustable vertical magnetic field on the order of several gauss. At the end of the excitation region the atoms enter a detector for the metastable $2S$ state. Inside a closed μ-metal cylinder with an entrance hole of diameter 5 mm, an electric field of approximately 100 V/cm mixes the $2S$ and $2P$ states and quenches the excited state. We detect the decay by monitoring the emission of Lyman-α photons with a solar blind photomultipler (Hamamatsu, R1459). At 243 nm the quantum efficiency is suppressed by a factor of 10^8 compared to the maximum efficiency of 10% near 121 nm. The MgF_2 window is shielded by a graphite coated net and the cathode is set to ground potential. With a solid angle of 0.72π and losses due to the shielding net and quench electrodes, we estimate a total detection efficiency of about 0.5%. Typical count rates at 79 K with 50-mW circulating uv power are 5×10^5 s^{-1}. The pulses from the photomultiplier are amplified (Le Croy 612A), discriminated (Le Croy 623B), and counted (Le Croy, scaler 2551) with commercial CAMAC modules. For data acquisition and laser frequency control we use an IBM-compatible personal computer.

III. SPECTRUM AND LINE SHAPE OF THE TWO-PHOTON RESONANCE

A. General remarks

According to the selection rules for a two-photon transition between S states ($\Delta L=0$, $\Delta F=0$, and $\Delta m_F=0$), the hydrogen $1S$-$2S$ transition consists of two components corresponding to the two possible values of the total angular momentum quantum number $F=1$ and 0. Because of their threefold degeneracy, the transition between the $F=1$ energy levels is 3 times stronger than the $F=0$ transition. In the case of deuterium with its nuclear spin quantum number $I=1$, the two hyperfine components ($F=\frac{1}{2}$ and $\frac{3}{2}$) are twofold and fourfold degenerate and thus show a line strength ratio of $\frac{1}{2}$. Since for both atoms the hyperfine splitting is very well known, we may restrict ourselves to the stronger component ($F=1$ and $\frac{3}{2}$, respectively).

The important feature of the two-photon excitation spectrum is a narrow Doppler-free peak due to absorption of the two photons from opposite directions. If relativistic effects are neglected, the linear Doppler shifts for both photons cancel and all atoms are resonant simultaneously, independent of their individual velocity. In addition, there is a Doppler-broadened pedestal originating from absorption of the two photons from the same direction. Since the Doppler width of typically several gigahertz exceeds the observed linewidth of the Doppler-free signal by a factor of approximately 10^5, the Doppler-broadened pedestal is insignificant and will be neglected in the following. At the light intensities typical in our experiment (100 W/cm^2) the corresponding Rabi frequency is on the order of 100 Hz. The interaction time is well below 1 ms even for cold atoms and thus saturation plays practically no role and may also be neglected in the calculation.

B. Shape of the resonance line

To analyze the shape of the resonance line we model the atomic beam as a flux of independent particles propagating on straight trajectories starting in a plane normal to the beam at the end of the nozzle and ending in plane of detection, 11.6 mm downstream. The frequency response of a single atom is determined by transit broadening and the relativistic Doppler effect. The resonance frequency of a moving atom is redshifted proportionally to v^2 when observed with a laser at rest in the laboratory frame, while the transit broadening depends only linearly on the atomic velocity v. Therefore, the average Doppler shift will decrease faster with temperature, leaving transit broadening the dominant effect at low temperatures. The most probable thermal velocity for hydrogen can be varied from 2230 m/s at 300 K, 1150 m/s at 79 K, down to 380 m/s at 8.7 K.

The density of atoms inside the nozzle may be estimatd from the measured pressure inside the discharge (between 0.5 and 1.5 mbar) and from the area and the length of the nozzle (4.5 mm$^2\times$2 mm). We find that the mean free path for the atoms inside the nozzle is comparable to the nozzle diameter; therefore we cannot totally exclude interatomic collisions inside the nozzle. Nevertheless, in our model we only regard atoms that start their flight at the nozzle wall and have completed their interaction with the laser beam before they reach the detector. This simplification allows for an approximate analytic expression of the flux F of excited atoms through the detector

(see the Appendix):

$$F=\frac{\pi^2}{4}|D_{ab}I|^2 N_d L \frac{w_0^3}{v_t} M(\Omega_0) , \quad (1)$$

with the dimensionless line-shape function

$$M(\Omega_0)=\left[1+\frac{\Delta r}{\Delta f}\mathcal{S}\right]^{-2}\{\exp(-|\Omega_0|/\Delta f) + A\exp(-|\Omega_0|/\Delta r)\} ,$$

where A and $\mathcal{S}$ are given by

$$A=\left[\frac{\Delta f-\Delta r}{\Delta f+\Delta r}\right]^2\left[1-\Omega_0\left[\frac{1}{\Delta r}+\frac{1}{\Delta f}\right]\right] - \left[1-\Omega_0\left[\frac{1}{\Delta r}-\frac{1}{\Delta f}\right]\right] ,$$

$$\mathcal{S}=-1 \text{ if } \Omega_0<0;\ A=0,\ \mathcal{S}=+1 \text{ if } \Omega_0>0 .$$

Here N_d denotes the atomic density in the detection plane, the detuning $\Omega_0=\omega-1/2\omega_{ab}$, w_0 is the waist of the laser beam, L describes the distance between nozzle and detector, and $|D_{ab}I|$ contains the two-photon transition matrix element and the light intensity I ($D_{ab}=4.63\times10^{-4}$ $\mathrm{W^{-2}m^2s^{-1}}$). The two independent fit parameters

$$\Delta r:=\frac{1}{2}\left[\frac{v_0}{c}\right]^2\omega$$

and

$$\Delta f:=\frac{v_t}{2w_0}$$

contain the parameters v_0 and v_t of the longitudinal and the transvese velocity distribution (see the Appendix). Δr and Δf may be interpreted as the average relativistic Doppler shift and the average transit-time broadening, respectively.

The theoretical line-shape function is fitted to the measured data by varying the amplitude, the overall amplitude offset, the frequency offset, and the two distribution parameters v_0 and v_t. The fit was performed by means of commercial data analysis software based on the Levenberg-Marquardt fit algorithm [22]. The set of parameters that minimizes this sum is used to determine the line strength and, most importantly, the resonance frequency for an atom at rest. In Figs. 10 and 11 we show the experimental data for hydrogen and deuterium together with the theoretical line shapes at various temperatures. Compared to hydrogen, the deuterium resonance is considerably sharper, as expected from the larger deuterium mass which reduces the thermal velocity by $\sqrt{2}$. The resonances recorded near liquid-helium tempearture are by far the best resolved hydrogen or deuterium resonances. The relative linewidth of 1 part in 10^{11} is even two orders of magnitude smaller than that of the hydrogen maser. By comparison with the theoretical line shape, one may determine the relativistic Doppler shift,

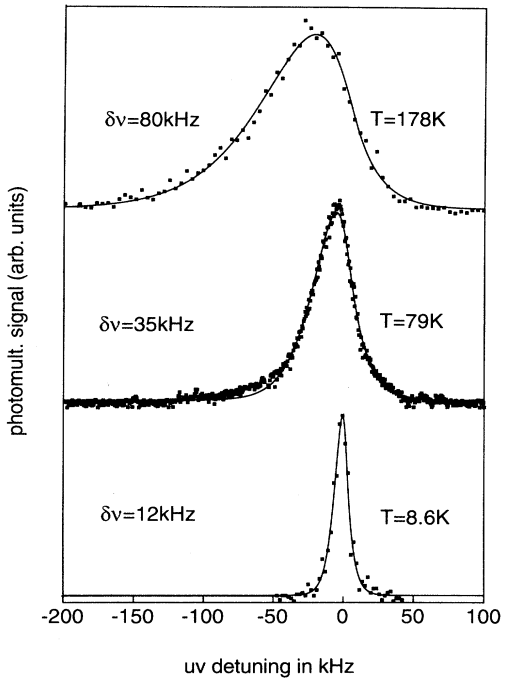

FIG. 10. Spectrum of the 1S-2S transition, $F=1$ component of atomic hydrogen at several temperatures.

i.e., the frequency by which the maximum of the resonance line is shifted to lower frequencies compared to the resonance frequency of an atom at rest. At 178 K this shift has a value of -21 kHz, while at 80 and 8.7 K it decreases to -5.7 and 0.5 kHz, respectively. We observe small discrepancies of the theoretical line shape from the measured data. They are caused by the restriction in the calculation to atoms that traverse the light beam completely. The observed discrepancies decrease for lower temperatures of the atomic beam.

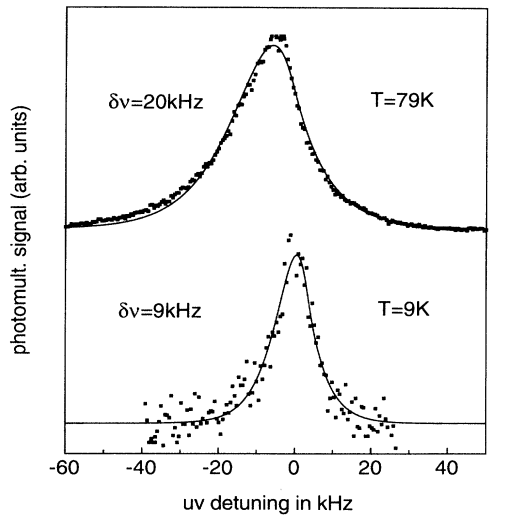

FIG. 11. Spectrum of the 1S-2S transition, $F=\frac{3}{2}$ component of atomic deuterium at 79 and 9 K.

An exact solution would require a numerical integration of the excitation probabilty along the trajectory of a single atom. Such a calculation is under preparation and may become important for future ultraprecise measurements in which the relativistic Doppler shift of the 1*S*-2*S* spectrometer contributes significantly to the systematic error.

At 8.7 K the signal drops to 700 s^{-1}, which is 10^{-5} of the expected rate. This dramatic decrease in signal strength at low temperatures is also observable in the signal of the mass spectrometer. It is caused by surface catalyzed hydrogen recombination inside the nozzle [21]. The resonance at 8.7 K has been recorded with the help of a chopper which blocks the uv light with a period of 0.1 ms. For data taken only during the dark period, the background noise from uv light scattering at the cavity mirrors is completely suppressed and the signal-to-noise ratio increases dramatically.

During the high-precision measurements [5,8,9] we lock the laser to the maximum of the 79 K resonance. This is done by the data acquisition computer. It computes the difference between the count rates at two frequencies separated by 4 kHz. The numerically determined derivative has a zero crossing at the maximum of the resonance and establishes a suitable error signal. With the servo loop closed, the drift of the reference resonator shows up directly in the frequency of the AOM, which is used to tune the laser relative to the reference resonator during the period shown in Fig. 12. The resonator drift of roughly 10 Hz/s can be observed. The fluctuations of the AOM frequency indicate the quality of the lock. For an averaging time of 10 s the statistical error of the servo loop falls well below 100 Hz and the total error is dominated by the uncertainty with which we are able to derive the position of the maximum relative to the resonance frequency of an atom at rest. We conservatively estimate this uncertainty to be 6 kHz at 79 K, which equals the total Doppler shift that we obtain by comparison with the line-shape function.

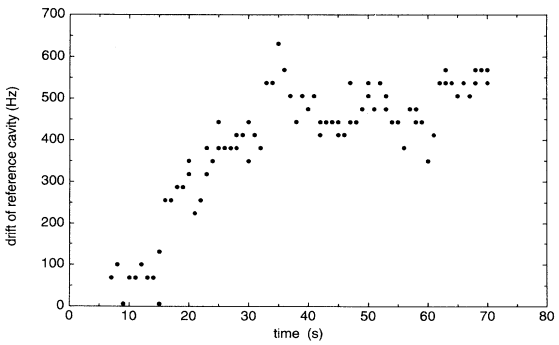

FIG. 12. Drift of the reference resonator. The dye laser is locked to the resonance of the hydrogen 1*S*-2*S* transition by means of a servo loop which controls the frequency separation between the reference resonator and the dye laser with an acousto-optic modulator (AOM). The change of twice the AOM frequency directly monitors the drift of the reference resonator.

IV. SYSTEMATIC EFFECTS ON THE 1*S*-2*S* TRANSITION FREQUENCY

A. Pressure shift

The pressure shift of the 1*S*-2*S* transition frequency is well known from previous hydrogen experiments by Beausoleil *et al.* [23]. Using the reported linear shift rate of 5.6 MHz/Torr, we calculate a shift on the order of 10 Hz at 243 nm.

B. Electric fields

A static electric field in the excitation region couples the $2S_{1/2}$ state to the $2P_{1/2}$ and $2P_{3/2}$ states and shifts the $2S_{1/2}$ level by $3.6E^2$ kHz cm^2/V^2 to higher energies. In addition, the lifetime of the $2S_{1/2}$ state is reduced to $\tau_{2S}=\tau_{2P}\ (E/475\ \text{V/cm})^{-2}$, with $\tau_{2P}=1.6$ ns. Since we still observe atoms with a time of flight on the order of 5×10^{-4} s (at 9 K), the survival of these atoms provides an upper limit for the electric field of 1 V/cm equivalent to a shift of 1.8 kHz. The actual electric stray field is probably much smaller. All surfaces near the excitation region have been coated with graphite spray. The flight path is additionally shielded by a graphite-coated cylindrical grid. As reported by Garreau *et al.* [24], the stray field expected for such an environment is on the order of 2 mV/cm. Even if oil diffusion pumps are used the electric stray field stays below 30 mV/cm. If we conservatively assume a value of 100 mV/cm, the shift of the 1*S*-2*S* resonance would be 180 Hz.

The ac Stark shift has been calculated in Ref. [28] to be $\Delta\nu=1.67I$ Hz cm^2/W for atoms excited on the passage through a Gaussian mode with intensity I. At 100 mW circulating power the intensity inside the uv resonator of $I=162$ W cm^{-2} shifts the transition to higher frequency by an amount of 271 Hz. Ionization from the 2*S* state to a continuum state additionally broadens the resonance by $1.8I$ Hz cm^2/W, i.e., 292 Hz at 100 mW.

C. Magnetic fields

We have studied the influence of a static magnetic field by means of a pair of coils mounted around the vacuum chamber. Figure 13 shows the transitions between the different Zeeman sublevels of the $F=\frac{3}{2}$ states in deuterium. The two components with $|m_F|=\frac{1}{2}$ and the ones with $|m_F|=\frac{3}{2}$ are clearly split at a magnetic-field strength of 8 G. The recorded data agree well with the predictions of the Breit-Rabi formula. For high-precision measurements we apply a magnetic field of several gauss that separates the different Zeeman components. Then we stabilize the laser frequency on the transition with $|m_F|=1$ ($|m_F|=\frac{3}{2}$ in the case of deuterium). The frequency of this component is nearly not shifted in a magnetic field. The small shift is due to the relativistic Zeeman effect, a small dependence of the electron g factor on the binding energy. This slits the $F=1$, $m_F=-1$, and $m_F=1$ components of the spectrum by approximately 36 Hz/G (at 243 nm), which is obviously of minor importance for the precision experiments described in the fol-

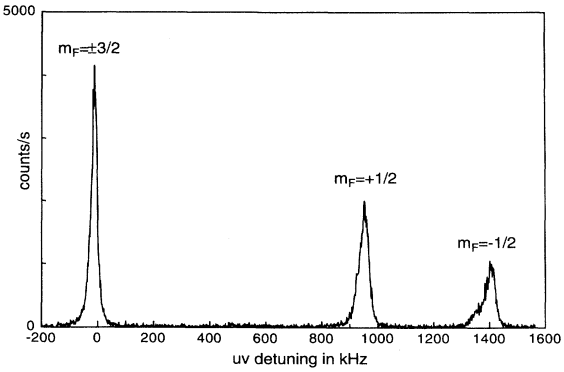

FIG. 13. Spectrum of the Zeeman sublevels $|m_F| = \frac{3}{2}$ and $\frac{1}{2}$, of the $1S$-$2S$, $F = \frac{3}{2}$ component of atomic deuterium (magnetic field 8 G, nozzle temperature 79 K).

lowing section. In the future, however, it may be interesting to observe this effect directly. A magnetic field of 300 G, necessary to observe this splitting, can be produced by water-cooled electromagnets.

V. HIGH-PRECISION MEASUREMENTS BASED ON THE 1S-2S SPECTROMETER

The above-described $1S$-$2S$ apparatus is part of a hydrogen project which was started in the MPQ in Garching in 1986. Other important parts of the project are a phase-coherent frequency chain and a beam apparatus for the observation of the $2S$-$4S$, D hydrogen two-photon resonances. Both have been constructed by different subgroups and are described elsewhere. The complete description of the whole project is clearly beyond the scope of this paper and, in the following, we will restrict ourselves to a brief review of the measurements and their results.

A. Isotope shift between the hyrogen and deuterium 1S-2S transition

For the isotope shift measurement a second dye laser similar to the one described above serves as an auxiliary frequency reference. This second laser is locked to the stable reference resonator and sidebands are superimposed at ±84 GHz by means of a fast electro-optical phase modulator [25]. The modulator frequency is phase locked to a rubidium frequency standard. If the reference laser is tuned halfway between the hydrogen and the deuterium resonance, the sidebands nearly coincide with the two atomic transition frequencies and the isotope shift may be derived from the beat signals between the sidebands of the reference laser and the laser we use to excite the transitions. Since we cannot observe hydrogen and deuterium simultaneously, the drift of the reference resonator during the time it takes to switch between the two isotopes turns out to be the main error source. During the measurement we alternate between hydrogen and deuterium and record the two beat signals versus time. For the missing data points during the time the laser excites the other isotope we interpolate with a polynomial of fourth order and finally correct for hyperfine structure and the different second-order Doppler effects. As the result we obtain an isotope shift of 670 994 337(22) kHz [4]. The theoretical prediction of 670 994 445(33) kHz combines reduced mass corrections, nuclear size effects, and a small correction due to the polarizability of the deuteron nucleus [26]. This 3σ discrepancy is probably due to an incorrect experimental value of the deuteron radius.

B. The 1S Lamb shift

A precise determination of the $1S$ Lamb shift without exact knowledge of the Rydberg constant is possible if the frequency of the $1S$-$2S$ transition is experimentally compared to four times the $2S$-$4S$, D transition frequency. Applying the simple Bohr model for the hydrogen atom one finds that both those frequencies should exactly coincide. The actually measured difference of 4836.136(10) MHz [5] is mainly due to relativistic and quantum electrodynamic corrections. A precise measurement leads to a substantially improved knowledge of the $1S$ Lamb shift.

The $2S$-$4S$ spectrometer used for this measurement [5] is based on a metastable beam of hydrogen or deuterium atoms in the $2S$ state. Similar to the $1S$-$2S$ spectrometer, a standing-wave cavity is placed inside a vacuum chamber. The standing light wave is parallel to the atomic beam. 60 W of circulating power stimulate a two-photon transition to the $4S$ or the $4D$ state from where the atoms rapidly decay to the ground state. The transition is detected as a signal drop of the metastable rate in a detector at the end of the excitation region and by detecting the fluorescence light of the $4S$-$2P$ decay at 486 nm with special fluorescence collecting optics. The excitation light is provided by a titanium sapphire laser at 972 nm, which is locked to a stable resonator similar to the one used in the $1S$-$2S$ experiment.

Part of the laser output is used to generate its second-harmonic frequency near 486 nm in a potassium niobate crystal. The doubled light is superimposed on a fast photodiode with light from the blue dye laser which is locked to the $1S$-$2S$ resonance. The weighted mean of the observed beat notes correspond to a $1S$ Lamb shift of 8172.86(6) MHz. Also at this level of accuracy one should take the QED two-loop corrections to the Lamb shift into account, which have recently been calculated [27].

C. Frequency of the hydrogen 1S-2S transition

The value of the $1S$-$2S$ transition frequency has been measured by comparison with the international time standard, i.e., the hyperfine transition of cesium. This was possible by means of a methane-stabilized helium neon laser near 3.39 μm, which serves as an intermediate standard. It was calibrated at the Physikalisch Technische Bundesanstalt in Braunschweig with a relative accuracy of 6×10^{-13}. The full accuracy is transported to the visible part of the spectrum by means of a phase-coherent frequency chain, which generates harmonic frequencies up to the eighth harmonic near 424 nm. In addition, we make use of a near coincidence between the hydrogen $1S$-$2S$ transition frequency and the fourteenth

harmonic of the methane resonance frequency. Therefore, if the frequency of the helium neon laser at 3.39 μm is added to the frequency of the dye laser near 486 nm in a nonlinear crystal, the resulting wavelength also happens to be near 424 nm and may be compared to eighth harmonic of the helium neon laser. Unfortunately, the coincidence is not perfect, and calibration of the dye laser with the full accuracy of the standard is only possible at 484 nm. To bridge the remaining difference of 2 nm the stable reference resonator is used whose longitudinal mode spacing has been calibrated to better than 1 Hz by means of the above-mentioned high-speed electro-optic modulator. The measured value for the hyperfine corrected $1S$-$2S$ transition frequency is 2 466 061 413.182(45) MHz [6]. We derive a value for the Rydberg constant of 109 737.315 684 4(31) cm^{-1} making use of the $1S$ Lamb shift measurement to correct for quantum electrodynamic effects [5], in excellent agreement with a more recently measured value of 109 737.315 683 4(24) cm^{-1} [10].

VI. CONCLUSION

In this paper we have described in detail our apparatus for spectroscopy on the $1S$-$2S$ transition of hydrogen in a cold atomic beam. About 450 mW of coherent light at 486 nm are produced by a single-mode dye laser that is pumped by a Kr^+ laser. The dye laser is stabilized with the Pound-Drever locking scheme to a highly stable reference cavity. The resulting linewidth of 2 kHz in 1 s is mainly limited by acoustic and seismic perturbations of the reference cavity. The output of the dye laser is resonantly enhanced in a passive bow-tie ring resonator, which contains a BBO crystal for generation of the second harmonic. We achieve an output of 10 mW at 243 nm. The uv light is coupled into an enhancement cavity inside a vacuum tank. A cold atomic beam, whose temperature can be controlled by changing the temperature of the copper nozzle from which it is emerging, is propagating parallel to the standing-wave field inside the uv cavity. On resonance some of the atoms are excited to the metastable $2S$ state. For detection the excited atoms are quenched in a small electric field. The resulting Lyman-α fluorescence is observed with a solar-blind photomultipler. The observed shapes of the resonance line at different nozzle temperatures were compared to an approximate expression for the shape of the resonance line.

ACKNOWLEDGMENTS

The frequency chain used for the absolute measurement of the $1S$-$2S$ transition was designed and built in collaboration with T. Andreae, D. Meschede, and R. Wynands. W. Vassen and A. Huber contributed substantially to the design of the $2S$-$4S$ spectrometer. R. Kallenbach invented the electrooptic microwave modulation scheme which was used for the isotope shift measurement. We thank H. Brückner, K. Linner, H. Mader, W. Simon, and F. Hunger (Coherent) for their expert technical assistance. It is a pleasure to thank K. Pachucki, A. Weis, and B. Neitzert for many helpful discussions. We would also like to thank E. Hagley for carefully reading the manuscript. Part of this work was supported by the Deutsche Forschungsgemeinschaft and within the frame of an EC SCIENCE program cooperation, Contract No. SCICT 92-0816.

APPENDIX: DERIVATION OF THE RESONANCE LINE-SHAPE FUNCTION

We start with an expression for the probability ρ to find an atom in the excited state as derived in Ref. [28] for a two-photon transition in the semiclassical approximation:

$$\rho := \rho_{aa}^{(2)}(t) = \exp(-\gamma t)\left| \int_{-\infty}^{t} dt' \frac{V_{ab}(t')}{\hbar} \exp\left[i\omega_{ab} t' + i\int_{-\infty}^{t'} dt'' \Delta\omega_{ab}(t'') + \gamma t'/2 \right] \right|^2 .$$

Here $h\omega_{ab}$ is the $1S$-$2S$ energy separation, $\Delta\omega_{ab}$ the ac Stark shift, and γ the decay rate of the $2S$ state. In the reference frame of the laboratory the interaction poential is given by

$$\frac{V_{ab}(t)}{\hbar} = D_{ab} \tfrac{1}{2} \varepsilon_0 c E_1(\mathbf{r},t) E_2(\mathbf{r},t) .$$

Here $D_{ab} = 4.63 \times 10^{-4}\ W^{-1} m^2 s^{-1}$ contains the transition matrix elements for the two-photon transition and E_1 and E_2 denote the electric fields of the two counterpropagating Gaussian waves inside the uv enhancement resonator. They have equal amplitude but opposite sign of the wave vector and thus

$$E_1(\mathbf{r},t) \cdot E_2(\mathbf{r},t) = E^2 e^{-2(r/w_0)^2} e^{-2i\omega t} .$$

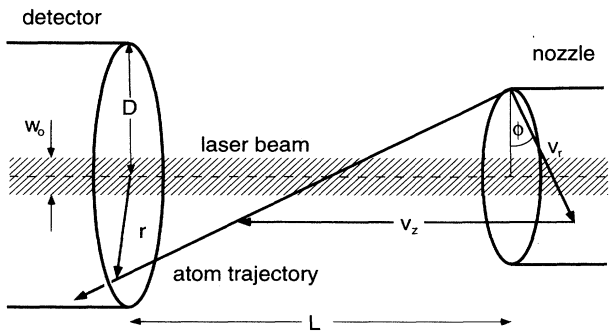

FIG. 14. Excitation geometry (for an explanation see the text).

The waist w_0 of the laser beam is assumed to be constant in diameter along the z axis and the geometrical phase shift is neglected. The electric-field amplitude E is given by the light intensity I at the center of the Gaussian beams:

$$I=\tfrac{1}{2}\varepsilon_0 cE^2=\frac{P}{\pi w_0^2} ,$$

where P is the circlating power inside the cavity.

Next we neglect the ac Stark shift $\Delta\omega_{ab}$ and transform V_{ab} into the reference frame of the atom by means of a Lorentz transformation, substitute it into the expression for ρ_{aa}, and carry out a second transformation back to the laboratory system. We neglect all terms of order $(v_r/c)^2$ and v_z/c^2 and find, for the excitation probability of an atom which has passed the light field on a particular trajectory,

$$\rho=|D_{ab}I|^2\left|\int_{t_i}^{t_f}d\tau\exp\left[-\frac{2}{w_0^2}[r^2+v_r^2\tau^2-2rv_r\tau\cos\phi]\right]\exp[-(2i\Omega+\gamma/2)\tau]\right|^2 \tag{A1}$$

with the detuning parameter Ω,

$$\Omega(v_z)=\omega\beta-\omega_{ab}/2\approx\Omega_0+\tfrac{1}{2}\omega\left[\frac{v_z}{c}\right]^2$$

and

$$\beta=\frac{1}{\sqrt{1-(v_z/c)^2}},\quad \Omega_0=\omega-\omega_{ab}/2 .$$

The trajectory of the atom is defined by its displacement r from the optical axis in the plane of the detector and by its velocity vector, which is expressed in cylinder coordinates (v_r, v_z, and ϕ; see Fig. 14). The integration limits t_i and t_f are established by the initial condition $\rho(t_i)=0$ when the atom leaves the nozzle and by the time of flight to the detector.

To obtain an analytic expression for the average flux of excited atoms through the detector we describe the geometry of the atomic beam, assuming two independent velocity distributions for the transverse and the longitudinal velocity component of the atoms v_r and v_z:

$$n_z(v_z)dv_z=\frac{4}{\sqrt{\pi}v_0^3}v_z^2\exp\left[\frac{v_z^2}{v_0^2}\right]dv_z ,$$

$$n_r(v_r)dv_r=\frac{2}{v_t^2}\exp\left[\frac{v_r^2}{v_t^2}\right]v_r dv_r .$$

The spatial distribution of the atoms is assumed to be homogeneous. The flux of excited atoms through the detector may be expressed as

$$F=N\int_0^\infty dv_z\int_{-\pi}^{\pi}d\phi\int_0^\infty dv_r\int_0^D r\,dr\,v_z n_z(v_z)n_r(v_r)\times\rho(v_r,v_z,\phi,r) . \tag{A2}$$

Here N is the density of atoms at the entrance plane of the detector and D is the radius of the entrance aperture of the detector. We also assume that all atoms have completely passed the light field before they are detected, i.e., that the trajectories start and end outside the laser beam. In this case the time integration limits may be extended to $t_i=-\infty$ and $t_f=\infty$. As a last simplification we use the decay rate γ to limit the time of flight and set $\gamma=v_z/L$, where L is the distance between the nozzle and the detector. The integral (A2) may be solved by first integrating over dr, $d\phi$, and dv_r. The time integration may be carried out in the limit $D\gg w_0$ and $\gamma\ll v_r/w_0$ by means of the integral theorem for Laplace transformations. The remaining integration over dv_z is straightforward and leads to Eq. (1).

[1] For an overview, see T. Kinoshita, *Quantum Electrodynamics, Advanced Series on Directions in High Energy Physics* (World Scientific, Singapore, 1990), Vol. 7.

[2] *The Hydrogen Atom,* edited by G. F. Basini, M. Inguscio, and T. W. Hänsch (Springer-Verlag, Berin, 1989).

[3] F. Schmidt-Kaler, Ph.D. thesis, University of Munich, 1992.

[4] F. Schmidt-Kaler, D. Leibfried, M. Weitz, and T. W. Hänsch, Phys. Rev. Lett. **70**, 2261 (1993).

[5] M. Weitz, A. Huber, F. Schmidt-Kaler, D. Leibfried, and T. W. Hänsch, Phys. Rev. Lett. **72**, 328 (1994).

[6] T. Andreae, W. König, R. Wynands, D. Leibfried, F. Schmidt-Kaler, C. Zimmermann, D. Meschede, and T. W. Hänsch, Phys. Rev. Lett. **69**, 1923 (1992); M. Weitz, F. Schmidt-Kaler, and T. W. Hänsch, *ibid.* **68**, 1120 (1992).

[7] C. Zimermann, R. Kallenbach, and T. W. Hänsch, Phys. Rev. Lett. **65**, 571 (1990).

[8] W. E. Lamb and R. C. Retherford, Phys. Rev. **72**, 241 (1947); **79**, 549 (1950); **81**, 222 (1951); S. R. Lundeen and F. M. Pipkin, Phys. Rev. Lett. **46**, 232 (1981); E. W. Hagley and F. M. Pipkin, *ibid.* **72**, 1172 (1994).

[9] R. S. van Dyck, Jr., P. B. Schwinberg, and H. G. Dehmelt, Phys. Rev. Lett. **59**, 26 (1987).

[10] F. Nez *et al.*, Phys. Rev. Lett. **69**, 2326 (1992).

[11] Yong-Shi Wu and Zi Wang, Phys. Rev. Lett. **57**, 1978 (1986).

[12] J. Hought, D. Hils, M. D. Rayman, Ma L.-S., L. Hollberg, and J. L. Hall, Appl. Phys. B **33**, 179 (1984); R. W. Drewer, J. Hough, G. M. Ford, A. J. Munley, and H. Ward, *ibid.* **31**, 97 (1983).

[13] A. Schenzle, R. G. DeVoe, and R. G. Brewer, Phys. Rev. A **25**, 2606 (1982).

[14] Coherent Inc. Technical manual CR-699, 1986 (unpublished).

[15] D. H. McIntyre, W. M. Fairbanks, Jr., S. A. Lee, T. W. Hänsch, and E. Riis, Phys. Rev. A **41**, 4632 (1990); G. P. Barwood, W. R. Rowley, P. Gill, J. L. Flowers, and B. W. Petley, *ibid.* **43**, 4783 (1991).

[16] J. Dirscherl, B. Neizert, T. Wegener, and H. Walther, Opt. Commun. **91**, 131 (1992); N. M. Sampas, E. K. Gustafson, and R. L. Byer, Opt. Lett. **18**, 947 (1993); J. C. Bergquist *et al.*, in *Light Induced Kinetic Effects on Atoms, Ions, and Molecules,* edited by L. Moi *et al.* (ETS Editrice, Pisa, 1991).

[17] D. Shoemaker, R. Schilling, L. Schnupp, W. Winkler, K. Maischberger, and A. Rüdiger, Phys. Rev. D **38**, 423 (1988).

[18] G. D. Boyd and D. A. Kleinman, J. Appl. Phys. **39**, 3597 (1968).

[19] H. Kogelnik and T. Li, Appl. Opt. **5**, 1550 (1966); H. Kogelnik, E. Ippen, A. Dienes, and C. V. Shank, J. Quantum Electron. **QE-8**, 373 (1972).

[20] T. W. Hänsch and B. Couillaud, Opt. Commun. **35**, 441 (1980).

[21] J. T. M. Walraven and I. F. Silvera, Rev. Sci. Instrum. **53**, 1167 (1982).

[22] W. H. Press *et al.*, *Numerical Recipes* (Cambridge University Press, Cambridge, 1988); proFit II, Quantum Soft, Zürich, Switzerland.

[23] R. G. Beausoleil, D. H. McIntyre, C. J. Foot, E. A. Hildum, B. Couillaud, and T. W. Hänsch, Phys. Rev. A **39**, 4591 (1989); M. G. Boshier, P. E. G. Baird, C. J. Foot, E. A. Hinds, M. D. Plimmer, D. N. Stacey, J. B. Swan, D. A. Tate, D. M. Warrington, and G. K. Woodgate, *ibid.* **40**, 6169 (1989).

[24] J. C. Garreau, M. Allegrini, L. Julien, and F. Biraben, J. Phys. (Paris) **51**, 2263 (1990).

[25] D. Leibfried, F. Schmidt-Kaler, M. Weitz, and T. W. Hänsch, Appl. Phys. B **56**, 65 (1993).

[26] K. Pachucki, D. Leibfried, and T. W. Hänsch, Phys. Rev. A **48**, R1 (1993); K. Pachucki, M. Weitz, and T. W. Hänsch, *ibid.* **49**, 2255 (1994).

[27] K. Pachucki, Phys. Rev. Lett. **72**, 3154 (1994).

[28] R. G. Beausoleil and T. W. Hänsch, Phys. Rev. A **33**, 1661 (1986).